

Spectroscopic triples and a chance alignment. A solution for a problem of suspicious mass ratios for SB2s from Wilson method.

Mikhail Kovalev,^{1,2,3}★ Xuefei Chen^{1,2,4} and Zhanwen Han^{1,2,4}

¹Yunnan Observatories, China Academy of Sciences, Kunming 650216, China

²Key Laboratory for the Structure and Evolution of Celestial Objects, Chinese Academy of Sciences, Kunming 650011, China

³Sternberg Astronomical Institute, M. V. Lomonosov Moscow State University, Leninskie Gory, Moscow 119991, Russia

⁴Center for Astronomical Mega-Science, Chinese Academy of Sciences, 20A Datun Road, Chaoyang District, Beijing 100012, China

Accepted XXX. Received YYY; in original form ZZZ

ABSTRACT

We selected three double-lined spectroscopic binary systems which have extreme mass ratios, if measured using the Wilson method. We analysed medium resolution spectroscopic observations and space-based photometry and find that all these systems are not SB2, but rather triple systems and a chance alignment of another star with SB1 that have an unseen component. Therefore suspicious mass ratios determined by the Wilson method for some double-lined spectroscopic binary systems aren't correct as these systems are more complex.

Key words: stars : fundamental parameters – binaries : spectroscopic – stars individual: J035146.75+252255.3, J061553.46+190014.8, J092306.86+431939.7

1 INTRODUCTION

Double-lined spectroscopic binaries are very useful astronomical objects since they allow us to estimate such important parameter as stellar mass. Mass ratio of the stellar components can be straightforwardly measured for such systems using a linear fit of the line-of-sight velocities $RV_{1,2}$, which is the so-called Wilson method (Wilson 1941). Unfortunately, this method sometimes produces extremely small or even nonphysical negative mass ratios (Kounkel et al. 2021).

Many double-lined spectroscopic binary (SB2) candidates were identified in Kovalev et al. (2022b) based on LAMOST (Large Sky Area Multi-Object fiber Spectroscopic Telescope) medium resolution spectra (MRS) (Liu et al. 2020). We arbitrary select three systems J035146.75+252255.3, J061553.46+190014.8 and J092306.86+431939.7 (hereafter j03, j06 and j09), where the Wilson method gives suspicious results, due to almost constant RV of the secondary spectral component. We list their literature info and designations in Table 1. The first one - j03 is known eclipsing binary, located near the Pleiades, although it is not a cluster member (Olivares et al. 2018). It has a single-lined spectroscopic (SB1) orbital solution in Gaia DR3 (Gaia Collaboration et al. 2022) and clear double-lined spectrum in LAMOST-MRS. The second one - j06 is actually two stars separated by $2.5''$ which were observed by the same fibre of LAMOST-MRS¹, so we can see the double-lined spectrum. The last one - j09 is the only system, where three spectroscopic components can be visually identified in the LAMOST-MRS

spectrum. Kounkel et al. (2021) found three spectral components in it's APOGEE DR16 spectrum (Ahumada et al. 2020). Recently it was identified as a spotted star using ASSAS-SN photometry by Christy et al. (2023) and analysed for ellipsoidal variability in TESS photometry by Green et al. (2023). We show the position of all three systems on Hertzsprung-Russell diagram in Figure 1, where they are all located higher than the main sequence for the field stars.

In this paper we use available LAMOST-MRS spectra and additional photometrical data to explore these systems. After detailed analysis we conclude that they are actually not SB2s, but spectroscopic triples j03, j09 and chance alignment of another star with j06 that have dark unseen component, possibly a white dwarf. The paper is organised as follows: in Section 2 we describe the observations. Section 3 presents our analysis and results. In Section 4 we discuss the results. In Section 5 we summarise the paper and draw conclusions.

2 OBSERVATIONS

2.1 Spectra

LAMOST (also known as Guo Shou Jing telescope) is a 4-meter quasi-meridian reflective Schmidt telescope with 4000 fibres installed on its 5-degree-FoV focal plane. These configurations allow it to observe spectra for at most 4000 celestial objects simultaneously (Cui et al. (2012); Zhao et al. (2012)). All available spectra for our three targets were downloaded from www.lamost.org. We use the spectra taken at a resolving power of $R = \lambda/\Delta\lambda \sim 7500$. Each spectrum is divided on two arms: blue from 4950 \AA to 5350 \AA and red from 6300 \AA to 6800 \AA . We convert the heliocentric wave-

★ E-mail: mikhail.kovalev@ynao.ac.cn

¹ fibre diameter is $\sim 3.3''$

star	j03	j06	j09
LAMOST Kovalev et al. (2022b)	J035146.75+252255.3	J061553.46+190014.8	J092306.86+431939.7
Gaia DR3 Gaia Collaboration et al. (2022)	66913361387671424	3373858954614854912 3373858958908468608	817543215158922368
G , mag	11.56	12.77 12.91	12.90
ϖ , mas	1.3215 ± 0.0295	1.2137 ± 0.0175 1.1445 ± 0.0248	2.8531 ± 0.0416
SB1 orbit			
P , d	5.73089 ± 0.00032		
t_0 , JD-2455197.5, d	-2.51583 ± 0.20445		
e	0.077 ± 0.029		
γ , km s ⁻¹	13.06 ± 0.92		
K , km s ⁻¹	44.46 ± 1.29		
ω , deg	195 ± 13		
Variable Star indeX Watson et al. (2006)	HAT 260-0002375 (EBA)		ASASSN-V J092306.83+431939.7 (ROT)
P , d	5.73382176		1.3137
Epoch HJD, d	2457063.8446		2458929.879
TESS input catalogue (TIC) Stassun et al. (2019)	84336450	718309429 718309430	99745836
ellipsoidal variability P , d Green et al. (2023)			1.301848

Table 1. Literature data compilation for the selected three systems. For j06 there are two sets of data in Gaia DR3 and TESS. EBA - eclipsing binary of Algol type, ROT - spotted star.

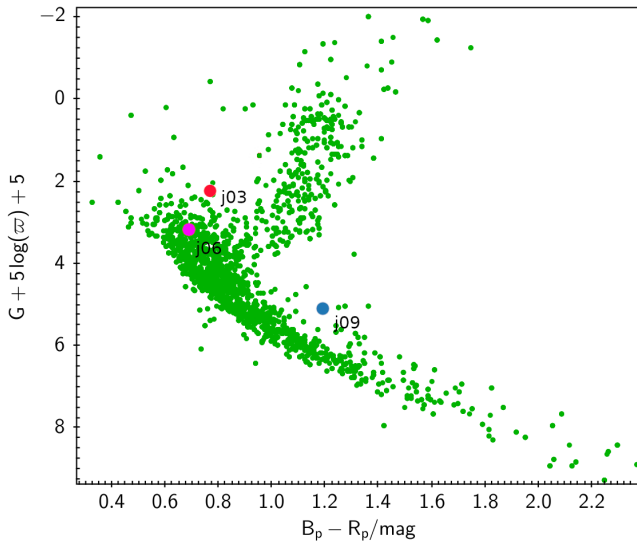


Figure 1. Hertzsprung-Russell diagram for all LAMOST MRS targets in the same field ($\sim 4^\circ$) with j09 (blue circle) based on [Gaia Collaboration et al. \(2022\)](#) data. j03 and j06 are shown as red and magenta circles respectively.

length scale in the observed spectra from vacuum to air using PyAstronomy ([Czesla et al. 2019](#)). For the short period ($P < 2$) systems j06 and j09, we analysed spectra taken during individual 20 minutes exposures, but for j03 we used spectra stacked for the whole night. In total we have 13, 60 and 63 spectra for j03, j06 and j09 respectively, where the average signal-to-noise ratio (S/N) of a spectrum ranges from 10 to 72 pix^{-1} for individual exposures and from 69 to for 240 pix^{-1} for stacked spectra.

2.2 Photometry

The Transiting Exoplanet Survey Satellite (TESS [Ricker et al. 2015](#)) mission observed all three systems, but for j03 there is high-quality light curve (LC) from Kepler K2 ([Barros et al. 2016](#)), which is available on the MAST portal², so we use it due to much higher precision. This LC covers time interval BJD=2457061:2457132 d. For j06 LCs are not available on the MAST portal yet, therefore we use eleanor ([Feinstein et al. 2019; Brasseur et al. 2019](#)) to extract the LC datasets from sectors 43, 44 and 45, covering the time interval BJD=2459474:2459551 d. We use default settings and slightly clip the edges of the LC, as they have some processing artifacts. For j09 we use TESS LC from sector 21 reduced by Quick Look Pipeline (QLP) ([Huang et al. 2020a,b](#)) and available on the MAST portal. This LC covers the time interval BJD=2458870:2458896 d.

3 METHODS AND RESULTS

3.1 Spectral analysis

Our spectroscopic analysis includes two independent stages:

- (i) analysis of individual observations by binary and single-star spectral models, where we normalise the spectra and make a rough estimation of the spectral parameters, see brief description in Section 3.1.1.
- (ii) spectral disentangling of the stacked spectra using FD3 code ([Ilijic et al. 2004; Ilijic 2017](#)), which is described in Section 3.1.2.

3.1.1 Individual spectra.

A detailed description of the spectral analysis is given in [Kovalev et al. \(2022b\)](#). In short, we used synthetic spectral models from

² <https://mast.stsci.edu/>

nlte.mpia.de, generated to be good representation of the single-star LAMOST-MRS spectra, see Appendix A. The normalised binary model spectrum is generated as a sum of the two Doppler-shifted normalised single-star model spectra $f_{\lambda,i}$ scaled according to the difference in luminosity, which is a function of the T_{eff} and stellar size. We assume both components to be spherical.

The observed spectrum is compared with model and normalised using `scipy.optimize.curve_fit` function. Each spectrum is fitted independently, unlike Kovalev et al. (2022a, 2023), as we are unable to put constraints on the mass ratio during the simultaneous multiple epochs fitting.

We show representative examples of our spectral fits for all three systems in Figure 2. As can be seen in all plots, the binary model is able to fit the observed spectrum much better than a single-star model, although for j09 a small contribution from a third component is also visible. Also note that for j09 we exclude the spectral region around the $H\alpha$ line as it has emission associated with the third component.

3.1.2 Spectral disentangling

Similarly to Kovalev et al. (2023) we use the Fourier spectral disentangling code FD3 by Ilijic (2017) for all three systems. This method requires clean spectra, without artefacts (i.e spikes from cosmic rays), thus we use it with stacked spectra. It can separate up to three spectral components and find the Keplerian orbit for an inner close binary. We use the blue and red spectral arms only for j03, while for j06 and j09 only the red arm is used. At first we try to separate the three spectral components for j06, but find no good solution, thus this system was analysed with only two components. For j03 and j09 we successfully find three components. For j06 and j09 we use light factors $LF = 1$ for all spectra, but for j03, thanks to the LC solution by JKTEBOP (see Section 3.3), we set LFs according to the light contribution of each component in the spectra. Therefore only for j03 spectral components are normalised to unity, while for j06 and j09 components the baseline is 1/2 and 1/3 respectively. We show the resulting spectral components in Figure 3 and list orbital solution's parameters in Table 2. As seen in the case of j03 all components have relatively narrow spectral lines, with the secondary component having deeper lines, but it's spectrum is too noisy as it contributes ~ 5 per cent of total light. In j06 the primary component has spectral lines with significant rotational broadening, while lines of the other component are relatively narrow. For j09 we can see emission in the $H\alpha$ line of the secondary, while this line is almost absent in the primary. Also note that spectral lines in the primary are more broadened than in the third component, which possibly rotates much slower. For all these plots we tried our best effort to remove smooth, kind-of-sinusoidal undulations in the spectral components, taking into account useful advice from Saša Ilijic (private communication) and Ilijic et al. (2004).

3.2 Orbital fitting

To get the orbital solution we select 13, 60 and 63 RVs of the primary components in j03, j06 and j09 respectively. We collect all RV measurements in Table B1 and use them to fit circular orbits with the generalised Lomb-Scargle periodogram (GLS) code by Zechmeister & Kürster (2009) :

$$RV_A(t) = \gamma - K_A \sin\left(\frac{2\pi}{P}(t - t_0)\right), \quad (1)$$

Table 2. FD3 orbital solutions for stacked spectra in the red arm. For j03 we also provide results for the blue arm spectrum. Unfortunately FD3 doesn't provide any uncertainties.

Parameter	j03	j06	j09
P , d	5.73128	0.47656	1.31059
(blue)	5.73157		
t_0 , HJD d	2458806.995	2458904.049	2458904.353
(blue)	2458806.378		
K_1 , km s $^{-1}$	62.96	44.63	83.94
(blue)	62.97		
K_2 , km s $^{-1}$	98.78		114.27
(blue)	100.69		
e	0.003	0.006	0.004
(blue)	0.001		
ω °	134.5	96.5	70.0
(blue)	96.3		

where γ - is the systemic velocity, P - is the period, t_0 - is the conjunction time, K - is the radial velocity semi-amplitude. We also fit to a Keplerian orbit and find that eccentricity is nearly equal to zero for all three systems, so a circular orbit is a valid assumption.

The circular orbit fit for j03 is shown in Figure 4. Note that the secondary spectral component has a blue shift relative to the systemic velocity. We show the orbital solutions for j06 and j09 in Figures 6 and 7. The agreement with a circular orbit is good, while RV data for the secondary spectral component are almost constant, with a slight red shift relative to systemic velocity. The radial velocities from Kounkel et al. (2021) also agree with our solution. For j09 there is a small signature of the Rossiter-McLaughlin (RM) effect (Rossiter 1924; McLaughlin 1924) around phase 1.0, although the RV uncertainties are too large to tell if it is real or not. High-resolution spectral observations can be very useful for this. Also the LC doesn't show any eclipse in this system, so the RM effect is very unlikely to be seen.

3.3 Light curves analysis

Among our three systems only LC for j03 shows eclipses (one of them is total, when the smaller component is completely hidden), thus we decide to model it using similar methods to ones in Kovalev et al. (2023). We used the JKTEBOP code (version 40)³ by Southworth (2013) to simultaneously fit the LC and RV timeseries in mode "task 3". Our fitting was initialised using P , t_0 , K , γ values from the GLS fit. We used limb darkening coefficients provided by the JKTLTD code and linearly interpolated them for spectral parameters of the primary: $T_{\text{eff}A} = 6300$ K, $\log(g) = 4.0$ dex, $[M/H] = -0.3$ dex. For the secondary component we set both coefficient to 0.3. We used quadratic limb darkening coefficients (LD). The gravity darkening coefficients were set to $\alpha = 0.32$ for both components. The reflection coefficients were computed based on system's geometry. The radial velocity was fitted for the primary component. Additionally we fit for a "third" light contribution L_3 , the nuisance parameter, the out-of-eclipse magnitude S_0 . In total we fit for 12 parameters: J the central surface brightness ratio, $(R_1 + R_2)/a$ the ratio of the sum of stellar radii to the semimajor axis, R_2/R_1 the

³ JKTEBOP is written in FORTRAN77 and the source code is available at <http://www.astro.keele.ac.uk/jkt/codes/jktebop.html>

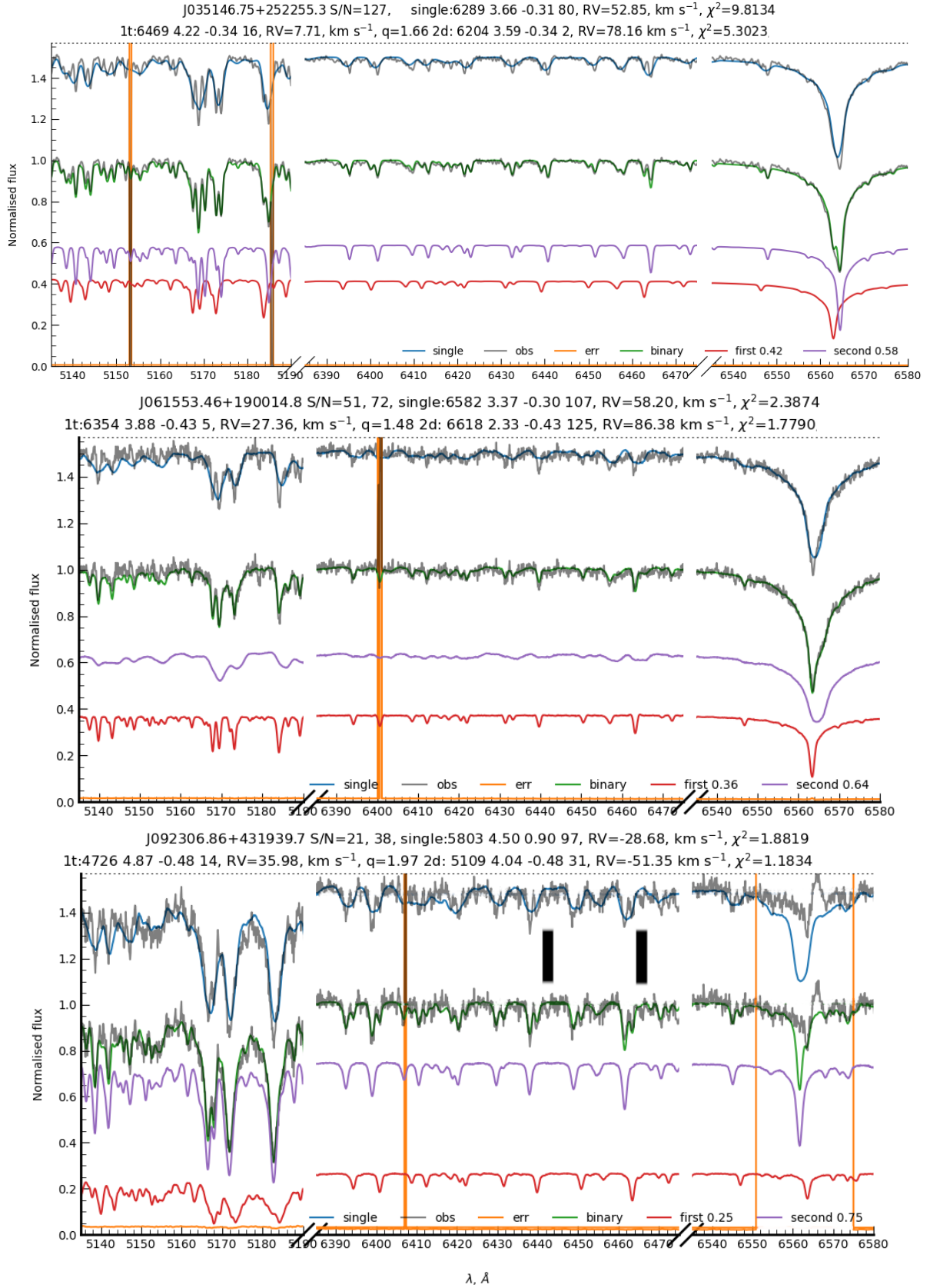


Figure 2. Example of the binary model (green line) and single-star model (blue line + 0.5 offset) fitting for LAMOST-MRS spectra for j03 (top), j06 (middle) and j09 (bottom). The observed spectrum and its error are shown as a gray and orange lines respectively. The primary component is shown as the purple line, the secondary as a red line. The third component is visible only for j09 as an emission line at H α and two weak lines at $\lambda = 6442, 6465$ Å (black blocks). Spectral parameters (T_{eff} , $\log(g)$, $[\text{Fe}/\text{H}]$, $V \sin i$) and RV from single star model fit and binary model fit are shown in the titles.

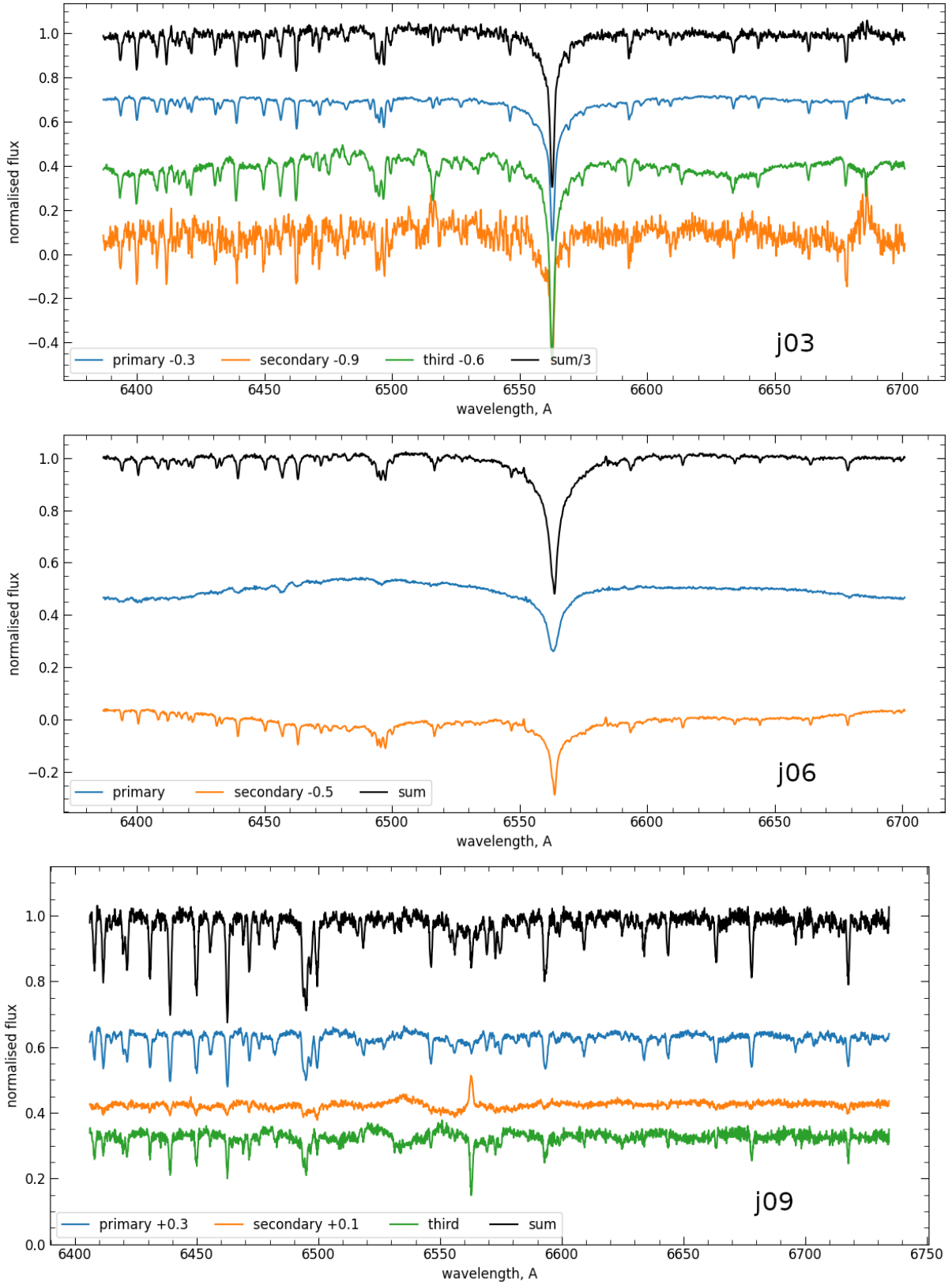
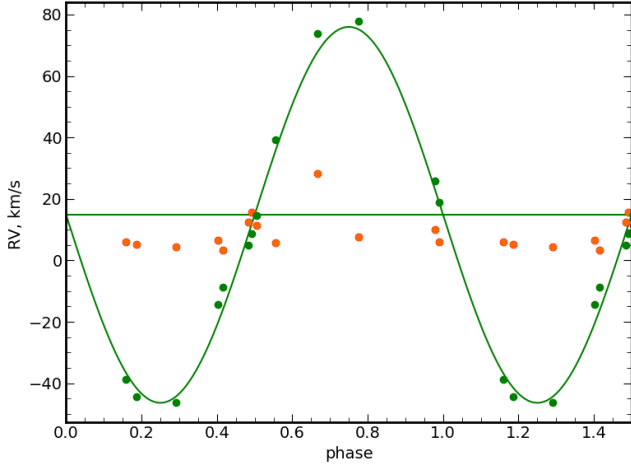


Figure 3. Example of the spectral separation for j03 (top), j06 (middle) and j09 (bottom). The total spectrum is shown as a black line. The primary component is shown as the blue line, the secondary as an orange line. The third component is shown as a green line.

star	j03	j06	j09
N_{RV}	13	60	63
P , d	5.730917 ± 0.001028	0.477201 ± 0.000002	1.310644 ± 0.000003
t_0 , HJD d	$2458806.301979 \pm 0.037755$	$2458496.584909 \pm 0.001147$	$2458468.635715 \pm 0.000843$
γ , km s^{-1}	14.81 ± 1.79	22.95 ± 0.72	32.69 ± 0.24
K , km s^{-1}	61.15 ± 2.53	68.60 ± 1.02	84.82 ± 0.34

Table 3. Orbital solutions with GLS.**Figure 4.** Circular orbit fit (green line) for the primary component (RV_1) of j03 (green circles). Note that the secondary spectral component (RV_2) (orange circles) has blue shift relative to the systemic velocity.**Table 4.** JKTEBOP solution for j03

Parameter	Value
fitted:	
J	0.636 ± 0.003
$(R_1 + R_2)/a$	0.179 ± 0.001
R_2/R_1	0.412 ± 0.009
i°	89.77 ± 2.35
$e \cos \omega$	-0.0001 ± 0.0001
$e \sin \omega$	-0.0050 ± 0.0001
P , d	5.73161 ± 0.00001
t_0 , HJD d	$2458806.25935 \pm 0.00353$
S_0 , mag	0.0006 ± 0.2515
L_3	0.399 ± 0.024
K_1 , km s^{-1}	62.39 ± 0.44
γ_1 , km s^{-1}	15.28 ± 0.38
fixed	
reflected light ₁ , mag	0.0006
reflected light ₂ , mag	0.0010
quadratic LD_1	0.2992, 0.3087
quadratic LD_2	0.3000, 0.3000

ratio of the radii, i the inclination, $e \cos \omega$, $e \sin \omega$ the eccentricity multiplied by the cosine and sine of the periastron longitude, P the period, t_0 , semi-amplitude and systemic velocity K_1 , γ_1 , L_3 and S_0 . We use integration ring size 1° . The best fit parameters are listed in Table 4 and Figure 5 shows the fit.

The LCs for j06 and j09 are folded with periods from the orbital

solution and shown in Figures 6 and 7. The photometrical data agree with the orbital solutions from the previous section. Changes in the LC are smaller than 3 per cent and there are no eclipses. The shape of the LCs suggests that the primary components in these two systems are non-spherical and significantly distorted by the tidal forces: the LC maxima correspond to $RV_{\min, \max}$ - moments when we can observe maximal projection of the primary component on the sky-plane. The LC minima have different depth: thus the primary's side facing the secondary is cooler due to gravitational darkening (highly likely for j06) or the secondary component reflects light from the primary (highly likely for j09). We leave detailed modelling of the LCs of these two systems for future studies.

Also we should note, that for j09 the data collected during TESS orbit 50 is very different from orbit 49, which can support the conclusion of Christy et al. (2023) that j09 is a spotted star. However it can be the same problem with data reduction (contamination and normalisation) as one mentioned in Kovalev et al. (2022a), where we decided to not use data from orbit 50 completely.

4 DISCUSSION

Analysis of these three systems confirms that the Wilson method cannot be applied to their RV measurements as they are not simple SB2. Below we will discuss them in detail.

4.1 j03

This system is a SB3 with significant difference in luminosity between components: the primary (~ 55 per cent) and secondary (~ 5 per cent) form an inner close binary subsystem with period $P \sim 5.73$ d, while the third component (~ 40 per cent) has an almost constant RV, with a slight blue shift ($\leq 10 \text{ km s}^{-1}$) relative to the systemic velocity of the inner system, see Figure 4, where it is shown as orange circles. This RV shift is small, so we think the third component is bound to the inner system. The simple two body orbital solution cannot capture the possible gravitational influence of third component, thus we recommend to use a more complex model in any future analysis of this system. If it is a triple system light-travel-time effect (Hajdu et al. 2022) should also be observed. We hope that such analysis will be done in future studies of this system, when longer time series will be available.

Thanks to spectral disentangling results for $K_{1,2}$ we can roughly estimate mass ratio in the inner subsystem $Q = K_1/K_2 \sim 0.63$. These results also allow us to roughly estimate the orbital semi-major axis a and the total mass $M_{\text{tot}} = (M_1 + M_2)$ using the Kepler's third law:

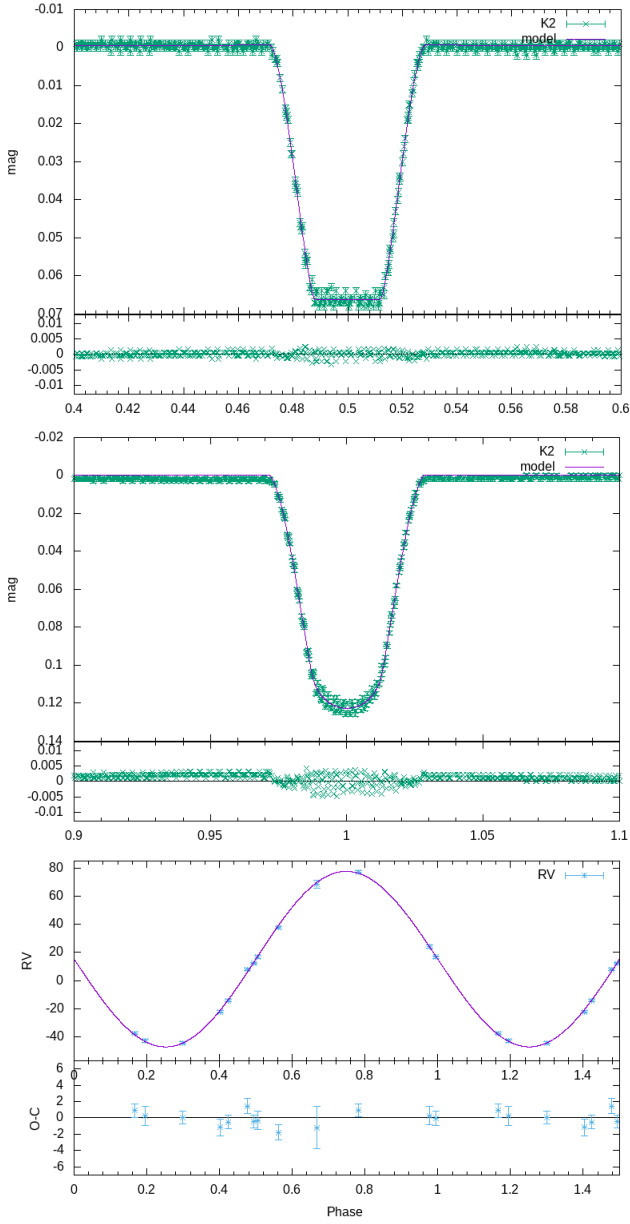


Figure 5. Best fit JKTEBOP model for j03. Top and middle panels show eclipses, bottom panel shows RV_1 .

$$a = (K_1 + K_2) \frac{P}{2\pi \sin i} = 0.085 \text{ [a.u.]} = 18.32 \text{ [} R_\odot \text{]}, \quad (2)$$

$$M_{\text{tot}} = \frac{(K_1 + K_2)^3 P}{GM_\odot \sin^3 i 2\pi} = 2.51 \text{ [} M_\odot \text{]}, \quad (3)$$

where $GM_\odot = 1.32712440041 \cdot 10^{20} \text{ m}^3 \text{ s}^{-2}$ is the Solar mass parameter⁴ and i is the inclination of the orbit to the sky-plane. Masses of the components can be found using total mass and Q : $M_{1,2} = 1.54, 0.97 M_\odot$. With the JKTEBOP solution we also make a rough estimation of the stellar sizes: $R_{1,2} = 2.32, 0.96 R_\odot$. Thus the secondary component is similar to the Sun, but it is completely

⁴ https://iau-a3.gitlab.io/NSFA/NSFA_cbe.html#GMS2012

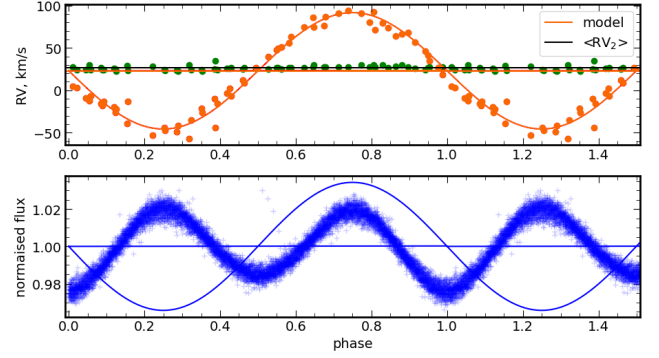


Figure 6. TESS LC for j06 folded with the period from orbital solution, which is schematically shown on the bottom panel. RV data (orange - RV_2 , green - RV_1) with best-fit circular orbit (top panel)

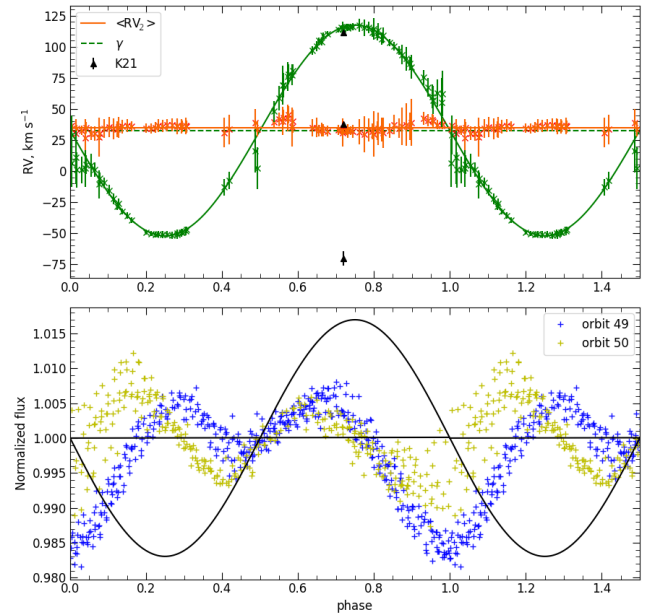


Figure 7. TESS LC for j09 folded with period from orbital solution, which is schematically shown on the bottom panel. RV data (green - RV_1 , orange - RV_2) with best-fit circular orbit (top panel). RV data from Kounkel et al. (2021) are shown as black triangles.

out-shined by other two stars in the spectrum. All these estimates are rough as we don't have an error value for K_2 and ignore the possible influence of the third component.

4.2 j06

The two visible spectral components belong to two stars separated by $2.5''$ observed by the same fiber of the LAMOST-MRS. In Gaia DR2 (Gaia Collaboration et al. 2018) both components had very similar parallaxes $\varpi_{1,2} = 1.1747 \pm 0.0476, 1.1744 \pm 0.0449$ mas, however recent Gaia DR3 values $\varpi_{1,2} = 1.2137 \pm 0.0175, 1.1445 \pm 0.0248$ mas suggest that the brighter component is a bit closer (~ 50 pc) to us, rejecting the possibility of them forming a wide system. We should note that $\langle RV_2 \rangle$ is very similar to the systemic velocity of the primary component (with red shift $\Delta RV \sim$

3.3 km s⁻¹). However proper motions from Gaia DR3 are quite different: $\mu_\alpha \cos \delta = 0.674 \pm 0.017$, 1.472 ± 0.023 mas yr⁻¹, $\mu_\delta = -3.924 \pm 0.013$, -4.271 ± 0.018 mas yr⁻¹ rejecting a possibility of j06 being a co-moving group of stars, which were born together. Thus we just have a chance alignment of SB1 and another star.

Using the orbital solution, the binary mass function can be calculated as follows:

$$f(M) = \frac{M_2 \sin^3 i}{(1+q)^2} = \frac{PK_1^3 (1-e^2)^{3/2}}{2\pi GM_\odot} = 0.0160 \pm 0.0007 [M_\odot], \quad (4)$$

where M_2 is the mass of the unseen star, $q = M_1/M_2$ is the mass ratio of this system, and i is the orbital inclination. By using the mass $M_1 = 1.489^{+0.040}_{-0.042} M_\odot$ of the visible star from Gaia DR3, we determined the minimum mass (taking $i = 90^\circ$) of the unseen object as $0.36 \pm 0.02 M_\odot$. Therefore we think that the unseen secondary is possibly a white dwarf.

Clearly visible ellipsoidal variability in the LC tell us that the primary component is significantly distorted by tidal forces. Spots are unlikely to cause such variability as it is very stable over full observation interval (150 periods) of this system by TESS, see Figure 6. Clear agreement between phased RV and LC time series also supports that variability is coming from the system in question, not from the other nearby stars observed by TESS.

4.3 j09

This system is the only one, where we can see three components, see Figure 2. Moreover, the secondary component has strong and stable emission in H α line, while this line is almost invisible in the primary, see the dynamic spectrum in the bottom panel of Figure 8. Also note that at phase $\phi = 0.25$ the primary has emission in H α . Such variable emission can support chromospheric activity of this component, which was also seen as spots by Christy et al. (2023). Like in j06, the third spectral component has a slight red shift relative to the systematic velocity ($\Delta RV \sim 2$ km s⁻¹), which can indicate that all three spectral components can form a large triple system. Unfortunately we didn't find any periodic changes in it's RV to confirm this hypothesis.

Thanks to the spectral disentangling results for $K_{1,2}$ we can roughly estimate the mass ratio of the inner subsystem $Q = K_1/K_2 \sim 0.73$. These results also allow us to make a rough estimation of a and M_{tot} :

$$a \sin i = (K_1 + K_2) \frac{P}{2\pi} = 0.024 \text{ [a.u.]} = 5.13 [R_\odot], \quad (5)$$

$$M_{\text{tot}} \sin^3 i = \frac{(K_1 + K_2)^3 P}{GM_\odot} = 1.06 [M_\odot], \quad (6)$$

Minimum masses of the components can be found using the total mass, Q and $i = 90^\circ$: $M_{1,2} = 0.61, 0.45 M_\odot$. Thus they are highly likely red dwarfs.

5 CONCLUSIONS

We selected three double-lined spectroscopic binary systems, which have extreme mass ratios, if measured using the Wilson method. The secondary spectral component in all of them has almost constant radial velocity. We analysed medium resolution spectroscopic observations from LAMOST-MRS and space-based photometry from

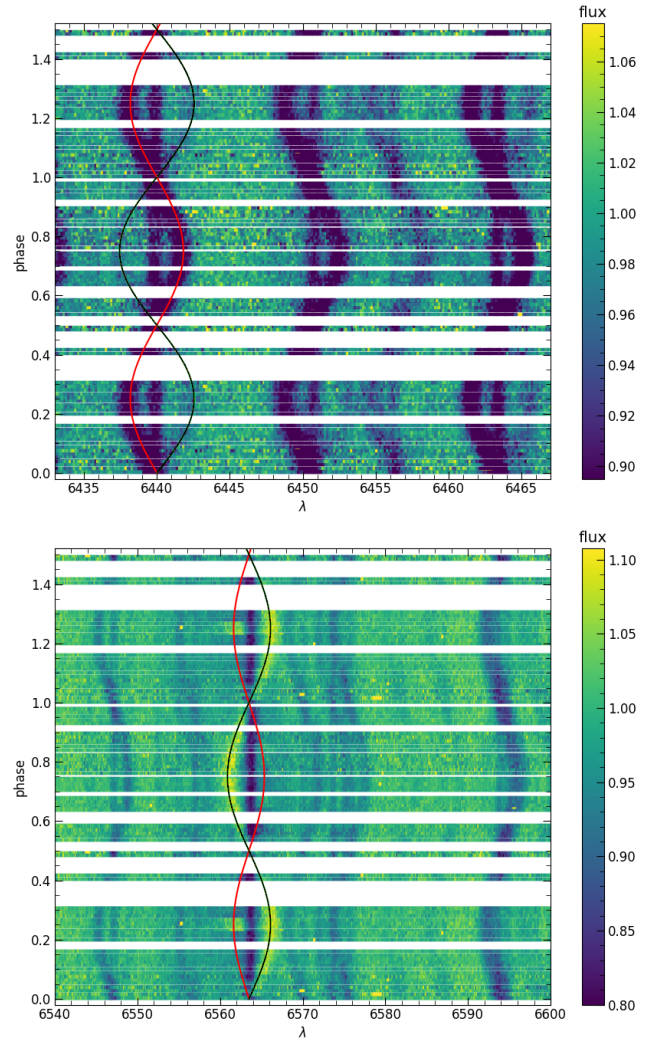


Figure 8. Dynamic spectrum of j09 in two regions of the red arm. The expected positions of the lines based on the orbital solution are shown with red (primary) and black (secondary) lines.

Kepler and TESS and find out, that all three systems are not simple SB2s, but rather triple systems and a chance alignment of another star with j06 that have an unseen component, possibly white dwarf. Thus we conclude that suspicious, extreme mass ratios measured using the Wilson method for SB2 systems are incorrect and these systems should be treated using more complex models.

ACKNOWLEDGEMENTS

We are grateful to the anonymous referee for a constructive report. We thank Hans Bähr for his careful proof-reading of the manuscript. We thank Saša Ilijić for help with FD3 code. We thank Hans Ludwig for useful discussion about nature of j09 system. MK is grateful to his parents, Yuri Kovalev and Yulia Kovaleva and to his aunt Elena Krivkina, for their full support in making this research possible. The work is supported by the Natural Science Foundation of China (Nos. 11733008, 12090040, 12090043, 11521303, 12125303, 12273057, 12288102). Guoshoujing Telescope (the Large Sky Area Multi-Object Fiber Spectroscopic Telescope LAMOST) is a National Ma-

for Scientific Project built by the Chinese Academy of Sciences. Funding for the project has been provided by the National Development and Reform Commission. LAMOST is operated and managed by the National Astronomical Observatories, Chinese Academy of Sciences. The authors gratefully acknowledge the “PHOENIX Supercomputing Platform” jointly operated by the Binary Population Synthesis Group and the Stellar Astrophysics Group at Yunnan Observatories, Chinese Academy of Sciences. This research has made use of NASA’s Astrophysics Data System, the SIMBAD data base, and the VizieR catalogue access tool, operated at CDS, Strasbourg, France. It also made use of TOPCAT, an interactive graphical viewer and editor for tabular data (Taylor 2005). Funding for the Kepler and TESS mission is provided by NASA’s Science Mission directorate. This paper includes data collected by the Kepler and TESS missions, which are publicly available from the Mikulski Archive for Space Telescopes (MAST). This work has made use of data from the European Space Agency (ESA) mission *Gaia* (<https://www.cosmos.esa.int/gaia>), processed by the *Gaia* Data Processing and Analysis Consortium (DPAC, <https://www.cosmos.esa.int/web/gaia/dpac/consortium>). Funding for the DPAC has been provided by national institutions, in particular the institutions participating in the *Gaia* Multilateral Agreement.

DATA AVAILABILITY

The data underlying this article will be shared on reasonable request to the corresponding author.

REFERENCES

- Ahumada R., et al., 2020, *ApJS*, 249, 3
- Barros S. C. C., Demangeon O., Deleuil M., 2016, *A&A*, 594, A100
- Brasseur C. E., Phillip C., Fleming S. W., Mullally S. E., White R. L., 2019, Astrocut: Tools for creating cutouts of TESS images, Astrophysics Source Code Library, record ascl:1905.007 (ascl:1905.007)
- Christy C. T., et al., 2023, *MNRAS*, 519, 5271
- Cui X.-Q., et al., 2012, *Research in Astronomy and Astrophysics*, 12, 1197
- Czesla S., Schröter S., Schneider C. P., Huber K. F., Pfeifer F., Andreasen D. T., Zechmeister M., 2019, PyA: Python astronomy-related packages (ascl:1906.010)
- Feinstein A. D., et al., 2019, *PASP*, 131, 094502
- Gaia* Collaboration et al., 2018, *A&A*, 616, A1
- Gaia* Collaboration et al., 2022, arXiv e-prints, p. arXiv:2208.00211
- Green M. J., Maoz D., Mazeh T., Faigler S., Shahaf S., Gorn R., El-Badry K., Rix H.-W., 2023, *MNRAS*, 522, 29
- Grupp F., 2004a, *A&A*, 420, 289
- Grupp F., 2004b, *A&A*, 426, 309
- Hajdu T., Matécsa B., Sallai J. M., Bódi A., 2022, *MNRAS*,
- Huang C. X., et al., 2020a, *Research Notes of the American Astronomical Society*, 4, 204
- Huang C. X., et al., 2020b, *Research Notes of the American Astronomical Society*, 4, 206
- Ilijic S., 2017, fd3: Spectral disentangling of double-lined spectroscopic binary stars, Astrophysics Source Code Library, record ascl:1705.012 (ascl:1705.012)
- Ilijic S., Hensberge H., Pavlovski K., Freyhammer L. M., 2004, in Hilditch R. W., Hensberge H., Pavlovski K., eds, *Astronomical Society of the Pacific Conference Series Vol. 318, Spectroscopically and Spatially Resolving the Components of the Close Binary Stars*. pp 111–113
- Kounkel M., et al., 2021, *AJ*, 162, 184
- Kovalev M., 2019, PhD thesis, IMPRS-HD, doi:10.11588/heidok.00027411
- Kovalev M., Li Z., Zhang X., Li J., Chen X., Han Z., 2022a, *MNRAS*, 513, 4295
- Kovalev M., Chen X., Han Z., 2022b, *MNRAS*, 517, 356
- Kovalev M., Wang S., Chen X., Han Z., 2023, *MNRAS*, 519, 5454
- Liu C., et al., 2020, arXiv e-prints, p. arXiv:2005.07210
- McLaughlin D. B., 1924, *ApJ*, 60, 22
- Olivares J., et al., 2018, *A&A*, 617, A15
- Ricker G. R., et al., 2015, *Journal of Astronomical Telescopes, Instruments, and Systems*, 1, 014003
- Rossiter R. A., 1924, *ApJ*, 60, 15
- Southworth J., 2013, *A&A*, 557, A119
- Stassun K. G., et al., 2019, *AJ*, 158, 138
- Taylor M. B., 2005, in Shopbell P., Britton M., Ebert R., eds, *Astronomical Society of the Pacific Conference Series Vol. 347, Astronomical Data Analysis Software and Systems XIV*. p. 29
- Ting Y.-S., Conroy C., Rix H.-W., Cargile P., 2019, *ApJ*, 879, 69
- Watson C. L., Henden A. A., Price A., 2006, *Society for Astronomical Sciences Annual Symposium*, 25, 47
- Wilson O. C., 1941, *ApJ*, 93, 29
- Zechmeister M., Kürster M., 2009, *A&A*, 496, 577
- Zhao G., Zhao Y.-H., Chu Y.-Q., Jing Y.-P., Deng L.-C., 2012, *Research in Astronomy and Astrophysics*, 12, 723

APPENDIX A: SPECTRAL MODELS

The synthetic spectra are generated using NLTE MPIA online-interface <https://nlte.mpia.de> (see Chapter 4 in Kovalev 2019) on wavelength intervals 4870:5430 Å for the blue arm and 6200:6900 Å for the red arm with spectral resolution $R = 7500$. We use NLTE (non-local thermodynamic equilibrium) spectral synthesis for H, Mg I, Si I, Ca I, Ti I, Fe I and Fe II lines (see Chapter 4 in Kovalev 2019, for references).

The grid of models (6200 in total) is computed for points randomly selected in a range of T_{eff} between 4600 and 8800 K, $\log(g)$ between 1.0 and 4.8 (cgs units), $V \sin i$ from 1 to 300 km s^{-1} and $[\text{Fe}/\text{H}]^5$ between -0.9 and $+0.9$ dex. The model is computed only if linear interpolation of MAFAGS-OS(Grupp 2004a,b) stellar atmosphere is possible for a given point in parameter space. Microturbulence is fixed to $V_{\text{mic}} = 2 \text{ km s}^{-1}$ for all models. The grid is randomly split on training (70%) and cross-validation (30%) sets of spectra, which are used to train *The Payne* spectral model (Ting et al. 2019). The neural network (NN) consists of two layers of 300 neurons each with rectilinear unit (ReLU)⁶ activation functions. We train separate NNs for each spectral arm. The median approximation error is less than 1% for both arms. We use output of *The Payne* as single-star spectral model.

APPENDIX B: RV MEASUREMENTS

We provide the RV measurements used to fit orbital parameters in Table B1.

This paper has been typeset from a $\text{\TeX}/\text{\LaTeX}$ file prepared by the author.

⁵ We used $[\text{Fe}/\text{H}]$ as a proxy of overall metallicity, abundances for all elements are scaled with Fe.

⁶ $\text{ReLU}(x) = \max(x, 0)$

Table B1. Radial velocity measurements for primary components. Full table is available online

time HJD d	value km s ⁻¹	error km s ⁻¹
j03		
2458802.242	-44.304	0.780
2458820.152	-14.188	0.817
2458830.141	-37.588	0.846
2458836.033	-42.888	1.171
2458852.089	16.806	0.880
2458883.994	37.598	0.965
2458890.986	77.144	0.780
2459124.326	12.263	0.784
2459148.249	68.523	2.610
2459181.120	-22.078	1.033
2459190.151	24.035	1.120
2459216.095	16.747	1.126
2459531.178	7.846	0.909
..